Available online at www.sciencedirect.com
SCIENCE DIRECT®
Journal of Magnetic Resonance 178 (2006) 142–154
JMR Journal of Magnetic Resonance
www.elsevier.com/locate/jmr

Linear response equilibrium

Kai W. Eberhardt, Michael Schär, Christoph Barmet, Jeffrey Tsao [1], Peter Boesiger, Sebastian Kozerke *

Institute for Biomedical Engineering, University of Zurich and Swiss Federal Institute of Technology, Zurich, Switzerland

Received 15 April 2005; revised 14 August 2005
Available online 13 October 2005

Abstract

A new periodic pulse sequence employing weak excitation is presented. This type of sequence drives the system into a steady-state with periodic time evolution from which the data can be reconstructed to a spectrum. It is demonstrated that the frequency response of such a sequence can be analyzed using perturbation methods and linear system analysis. A mathematical framework is proposed allowing the frequency response to be tailored by weighting a periodic flip function. The weak excitation level used implies very low specific absorption rates while generating a highly frequency selective signal in the order of $1/T2$ with signal strengths comparable to those obtainable with conventional large flip angle balanced steady-state free precession techniques. The concept is illustrated with phantom experiments and in vivo feasibility of water fat separation is shown on human knee images.

Keywords: Steady-state free precession; Frequency-selective imaging; Rapid imaging; Specific absorption rate; Small flip angle

1. Introduction

Spectrally sensitive imaging methods aim at separating resonances of different chemical shift. Conventionally, spectral selectivity is achieved by modifying the frequency response of the excitation pulse or by using frequency selective saturation or inversion prior to standard imaging experiments. Binominal and delays alternating with nutations for tailored excitation (DANTE) pulses [1] have been used for this purpose. High spectral selectivity, however, requires long pulse durations which compromise the signal-to-noise ratio (SNR) efficiency of the experiment.

A different approach is to resolve different spin frequencies by collecting multiple data points during signal evolution as done in chemical shift imaging (CSI). This requires an additional dimension to be recorded, resulting in longer measurement times. An overview and a comparison of CSI methods are given by Pohmann et al. [2].

Yet another approach is to exploit the spectral selectivity of the imaging experiment itself. Balanced steady-state free precession (SSFP) [3,4] techniques have recently enjoyed resurgence with faster gradient technology allowing shorter repetition intervals and thus more robust off-resonance performance. Sequences of equidistant radio frequency (RF) pulses of varying amplitude (OSSFP) [5] and phase (FEMR) [6] have been presented as a means to suppress spectral regions. Images acquired with different excitation frequencies have been linearly combined to achieve spectrally selective contrast (LCSSFP) [7,8]. In another approach phase sensitive reconstruction has been shown to allow separation of certain frequencies such as water and fat [9].

Pulse sequence design is closely related to radio frequency (RF) pulse design. By decomposing an RF pulse into smaller sub-pulses, the small-tip angle approximation [10,11] may be applied which offers an analytical and straightforward approximation technique to designing pulses. When considering a sequence of equidistant RF

* Corresponding author. Fax: +41 1 255 4506.
E-mail address: kozerke@biomed.ee.ethz.ch (S. Kozerke).
[1] Present address: Novartis Institutes for BioMedical Research Inc., Cambridge, MA, USA.

1090-7807/$ - see front matter © 2005 Elsevier Inc. All rights reserved.
doi:10.1016/j.jmr.2005.09.005

pulses with signal readouts in-between the pulses, the correspondence with DANTE experiments can be observed [1,12,13]. In DANTE experiments, however, the transient rather than the steady-state signal is excited.

This work proposes a mathematical framework which allows designing periodic low flip-angle pulse sequences for steady-state excitation to a desired frequency response. For this purpose, an approximate solution to the Bloch equations is derived with perturbation methods following ideas presented by Hoult [10] for designing RF pulses. It is shown that the steady-state response of the system can be linearly approximated very accurately at low flip angles. The frequency response can be controlled by modulating the train of flip angles, referred to as the flip function hereafter. We call this method linear response equilibrium (LRE).

In phantom experiments it is demonstrated that multiple resonance lines can be excited simultaneously and separated. In vivo feasibility of water fat separation is illustrated with images of a human knee.

2. Theory

2.1. Weak and strong excitation

To understand the response of a spin to a steady-state sequence it is conductive to consider an infinitely long excitation of a single frequency about the x-axis of the rotating frame. There are two different boundary cases of excitation to discern. If the excitation is comparable to excitation strengths used in continuous-wave (CW) NMR [14] the response of the system is given by a Lorentzian peak with absorption in the y-direction and dispersion in the x-direction (Fig. 1A). Under very strong excitation the peak will saturate and disappear during the transient state, while the signal of the dispersive component will saturate around the excitation frequency and increase at frequencies further from the excitation frequency (Fig. 1B). The direction of the signal for weak to strong excitation shows substantially different characteristics, although the phase is independent of the excitation. While the weak excitation generates signal from a small spectral region centered about the excitation frequency ω_0, the signal from the strong excitation is shifted to frequencies further away from ω_0. The magnetization of the narrow spectral region about the excitation frequency ω_0 is dephased. This spectral region is referred to as a darkband hereafter.

Infinitesimal hard pulses have no accentuated frequency in themselves, all frequencies are excited likewise. If one replaces the continuous excitation with infinitesimal hard pulses separated by the repetition time TR, two spins with frequencies separated by 1/TR will show the same behavior. Therefore, in the weak excitation case, the frequency response will be a comb of peaks separated by 1/TR (Fig. 1C). The response in the strong excitation case will show the well-known SSFP characteristics of wide passbands of high signal and narrow stopbands or darkbands where the magnetization is dispersed, periodic with 1/TR in the frequency domain at the echo time of TR/2 after a pulse (Fig. 1D). Ignoring motion and diffusion effects the excitation is unaffected by readout gradients in-between the pulses, since the gradients integrate to zero over each TR in balanced SSFP imaging.

2.2. Perturbation ansatz

In the following the response to continuous excitation is described using a perturbation approach. The Bloch equations written in complex form are

$$\begin{aligned}\frac{\mathrm{d}}{\mathrm{d}t}M_{xy}(t) &= aM_{xy}(t) + \varepsilon b(t)M_z(t)\\ \frac{\mathrm{d}}{\mathrm{d}t}M_z(t) &= Im(\mathrm{i}\varepsilon b(t)M_{xy}(t)) - \frac{M_z(t)-M_o}{T1}\end{aligned} \tag{1}$$

with $a = -1/T2 + \mathrm{i}\Delta\omega$, $\varepsilon b(t) = -\mathrm{i}\omega_{xy}(t)$, and $b(\mathrm{t})$ representing the perturbation of the system. $T1$, $T2$, $M_{xy} = M_x + \mathrm{i}M_y$, M_z and M_0 denote longitudinal and transversal relaxation times, and transverse, longitudinal and equilibrium magnetization, respectively. M_x and M_y are the transverse magnetization components along the x- and y-axis of the rotating frame. $\Delta\omega$ is the frequency offset of the spin in the rotating frame and $\omega_{xy}(t) = \omega_x(t) + \mathrm{i}\omega_y(t)$ describes how the spin is rotated by the RF, with $\omega_x(t)$ and $\omega_y(t)$ denoting the rotation about the x- and the y-axis. $Im()$ indicates that only the imaginary component of the function in the brackets is taken. The solution to Eq. (1) can be expressed as a power series of the following form:

$$M_{xy}(t) = \sum_{m=0}^{\infty} M_{xy}^{(m)}(t)\varepsilon^m, \quad M_z(t) = \sum_{m=0}^{\infty} M_z^{(m)}(t)\varepsilon^m. \tag{2}$$

Ordering the equations by order of ε results in:

$$\begin{array}{ll}\frac{\mathrm{d}}{\mathrm{d}t}M_{xy}^{(0)}(t) = aM_{xy}^{(0)}(t) & \frac{\mathrm{d}}{\mathrm{d}t}M_z^{(0)}(t) = -\frac{M_z^{(0)}(t)}{T1} + \frac{M_o}{T1}\\ \frac{\mathrm{d}}{\mathrm{d}t}M_{xy}^{(1)}(t) = aM_{xy}^{(1)}(t) + b(t)M_z^{(0)}(t) & \frac{\mathrm{d}}{\mathrm{d}t}M_z^{(1)}(t) = Im(\mathrm{i}b(t)M_{xy}^{(0)}(t)) - \frac{M_z^{(1)}(t)}{T1}\\ \vdots & \vdots\\ \frac{\mathrm{d}}{\mathrm{d}t}M_{xy}^{(m)}(t) = aM_{xy}^{(m)}(t) + b(t)M_z^{(m-1)}(t) & \frac{\mathrm{d}}{\mathrm{d}t}M_z^{(m)}(t) = Im(\mathrm{i}b(t)M_{xy}^{(m-1)}(t)) - \frac{M_z^{(m)}(t)}{T1}\end{array} \tag{3}$$

These equations can be solved sequentially. In this chapter only the results are presented, the full calculations can be found in Appendix A.

The zeroth order describes the behavior of the free unperturbed system:

$$\begin{aligned}M_{xy}^{(0)}(t) &= 0,\\ M_z^{(0)}(t) &= M_0\end{aligned} \tag{4}$$

with the initial conditions: $M_{xy}^{(m)}(t=0) = 0$, $M_z^{(0)}(t=0) = M_0$, $M_z^{(n)}(t=0) = 0$ for all integers $n \geqslant 1$ and $m \geqslant 0$.

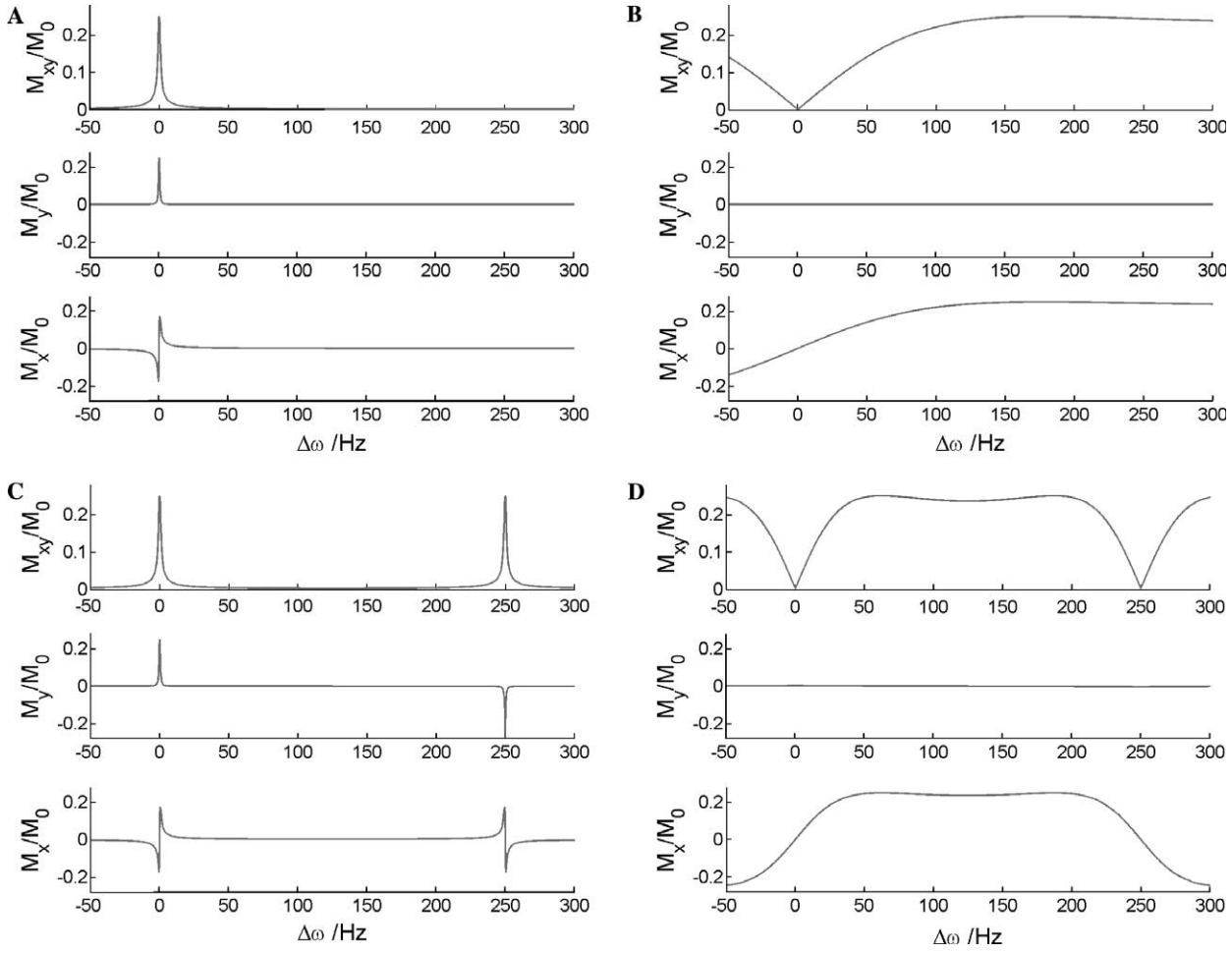

Fig. 1. Excitation profiles: (A) continuous weak excitation, 57.3°/s, this profile corresponds to the excitation profile excited in CW experiments; (B) continuous strong excitation, 28650°/s, the peak at $\Delta\omega = 0$ is saturated and the dispersion relation excites frequencies far from the excitation frequency; (C) darkband SSFP, the small flip-angle excitation is similar to that of weak CW excitation (A), but the profile becomes periodic with 1/TR, flip angle: 0.23° (optimal darkband flip angle, TR = 4 ms, TE = 2 ms); (D) SSFP without phase-alternation, the signal is in the x-direction of the rotating frame, as in CW strong excitation, but is periodic with 1/TR due to the pulsed excitation, flip angle 39° (optimal SSFP flip angle, TR = 4 ms, TE = 2 ms). Relaxation times are $T1 = 2$ s, $T2 = 0.5$ s.

The first order equations are the linear response to the perturbation

$$M_{xy}^{(1)}(t) = M_0 \sum_{\Omega} \frac{b_\Omega}{\mathrm{i}\Omega - a}(\mathrm{e}^{\mathrm{i}\Omega t} - \mathrm{e}^{at})$$
$$M_z^{(1)}(t) = 0 \tag{5}$$

with $b(t) = \sum_\Omega b_\Omega \mathrm{e}^{\mathrm{i}\Omega t}$ being the Fourier series of the perturbation, which is proportional to the Fourier series of the rotation of the spin by the RF flip function

$$\omega_{xy}(t) = \sum_{\Omega} \omega_\Omega \mathrm{e}^{\mathrm{i}\Omega t}, \tag{6}$$

where $\omega_\Omega = \mathrm{i}\varepsilon b_\Omega$. The index Ω is an abbreviation for $\Omega = 2\pi n/\mathrm{TS}$ with n being an integer. In case the RF is not periodic, the Fourier series can be replaced by the Fourier transformation.

The second order of M_{xy} is

$$M_{xy}^{(2)}(t) = 0. \tag{7}$$

Combining Eqs. (4)–(6), the response of the system up to the second order is

$$M_{xy}(t) \approx M_{xy}^{(0)}(t) + M_{xy}^{(1)}(t)\varepsilon^1 + M_{xy}^{(2)}(t)\varepsilon^2 = \sum_{\Omega} C_\Omega(\mathrm{e}^{\mathrm{i}\Omega t} - \mathrm{e}^{(-\frac{1}{T2}+\mathrm{i}\Delta\omega)t}) \tag{8}$$

with

$$C_\Omega = M_0\omega_\Omega \frac{-\frac{1}{T2} + \mathrm{i}(\Omega - \Delta\omega)}{\frac{1}{T2^2} + (\Omega - \Delta\omega)^2}.$$

This equation describes a sum of Lorentzian distributions C_Ω weighted by two rotating terms. The first term is the steady-state, and the second term describes the transient behavior, which decays exponentially with $T2$.

In the next section, it is shown that by applying the perturbation with hard RF pulses which have a periodically modulated amplitude, it is possible to create a ω_{xy} with a

selected number of Fourier coefficients, which, according to Eq. (8), excite the selected number of Lorentzian peaks C_Ω in the frequency domain.

2.3. Discretization of flip function

If the RF is applied in a pulsed fashion, data can be acquired with fully balanced gradients between pulses, without affecting the steady-state. If RF pulses are of very short duration their frequency-selectivity need not to be taken into account and they can be treated as infinitesimal, δ-like pulses.

Eq. (8) describes the behavior of the system in linear approximation. The response is easily illustrated for the simple case with a few peaks C_Ω being excited by continuous excitation. In an experiment, however, continuous excitation is not possible as data can only be acquired during time intervals where the RF transmitter is blanked.

If the flip function Eq. (6) consists of infinitely short δ-pulses at a repetition rate TR (Fig. 2A), the rotation about the x and y-axes is given by

$$\omega_{xy}(t) = \alpha(t) \sum_{i=0}^{\infty} \delta(t - i\mathrm{TR}). \tag{9}$$

We choose the flip-function to have a periodicity of TS with TS/TR = N being an integer. This is not necessary for the excitation, but the periodicity of the response allows for a segmented k-space acquisition in the experiment. Based on the convolution theorem, frequencies smaller than 1/TR of $\alpha(t)$ will be convolved around the frequencies of the δ-comb and frequencies higher than 1/TR will be aliased to a different frequency shifted by an integer multiple of 1/TR. The minimal distance between two peaks is 1/TS. An example of a flip function composed of infinitesimal hard pulses is derived in Appendix B.

2.4. Flip function design

To excite a desired steady-state response, the corresponding flip-function must be chosen. The number of peaks m is selected and $\omega_\Omega \exp(\mathrm{i}\Omega t)$ is added to the flip function $\omega_{xy}(t)$ for each peak at frequency Ω to be included. In a practical setting all frequencies Ω are excited with identical strength α_0 to account for field-inhomogeneities in the object. If the spectral region to be excited is chosen to be symmetric around the frequency

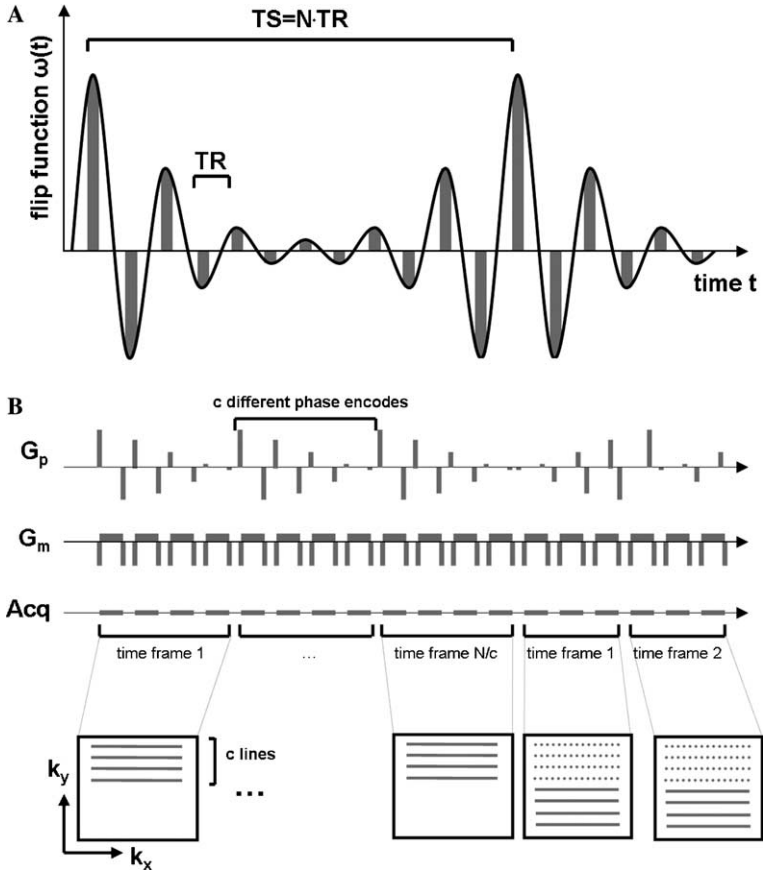

Fig. 2. Flip function and data acquisition. A flip function $\omega(t)$ of periodicity TS (A) is applied resulting in a comb of excited frequencies with a density of 1/TS given that excitation remains weak. Discrete sampling of the flip function every TR causes a periodicity of 1/TR of the excited comb. For spatial encoding, fully balanced readout- and phase-encode gradients are used which are denoted G_m and G_p, respectively (B). During TS, c different lines of k-space are sampled repeatedly m times with c denoting the spectral field-of-view reduction factors. Accordingly, spectral information from N/c peaks can be obtained. In the example illustrated c was set to four.

of the rotating frame of reference, the flip function becomes a sum of cosine functions. Hence $\omega_{xy}(t)$ reads as follows:

$$\omega_{xy}(t) = \alpha_0 \sum_{j=-(m-1)/2}^{(m-1)/2} \cos\left(\frac{2\pi}{\mathrm{TS}} jt\right) \sum_{i=0}^{\infty} \delta(t - i\mathrm{TR}) \qquad (10)$$

Accordingly, a uniform comb of m frequencies with density 1/TS is excited within the spectral field-of-view 1/TR.

2.5. Data acquisition and reconstruction

After acquisition, the spectral information must be deconvolved from the time evolution of the excited interval. To resolve m excited peaks, magnetization is sampled m times over the periodicity of the flip function TS using fully balanced gradients for spatial encoding as depicted in Fig. 2B. Spectral information is extracted using a discrete Fourier transformation as derived in Appendix C.

To account for field-inhomogeneities, TS is chosen to be approximately $T2$ of the sample. Thereby, images of an interval of frequencies wide enough to accommodate for field inhomogeneities may be reconstructed. Images may either be composed by superposing the absolute values or only the absorptive component of the peaks and thereby eliminating much of the unwanted signal from the passbands. This is analogous to looking at only the absorption-mode spectrum compared to the absolute-value spectrum.

2.6. Reduction of the spectral field-of-view

As the design of the flip function fully determines the density and number of excited peaks, the flip function and data acquisition strategy may be modified to allow a reduction of the number of excited peaks. Thereby the scan-time can be reduced without sacrificing spectral resolution, i.e., one can excite only a fraction of the maximally possible spectral field-of-view of 1/TR. If $N = \mathrm{TS}/\mathrm{TR}$ denotes the maximum number of peaks that can be excited, one may choose to excite only a subset of $m = N/c$ neighboring peaks with c denoting the reduction factor of the spectral field-of-view. In this case k-space must be filled in a segmented fashion as illustrated in Fig. 2B.

In data reconstruction, the evolution of the steady-state has to be compensated for prior to Fourier transformation. A detailed derivation is given in Appendix C.

3. Methods

3.1. Simulation

To validate that the response of the system using hard pulses is described by the perturbation solution a simulation was performed. The system response to hard pulses, described by rotational matrices, the second order and the third order analytical perturbation solutions are compared for $T1 = 2000$ ms and $T2 = 500$ ms (Fig. 3).

It can be shown that the approximation holds well for weak excitation using flip angles smaller than $\alpha_0 = \frac{\mathrm{TR}}{\sqrt{T1 \cdot T2}}$ [rad]. At these low flip angles the transverse magnetization reaches its maximal value in the direction of the absorptive signal component and is in excitation strength comparable to rates of CW NMR. The perturbation simulation only includes peaks within the shown 1/TR frequency-FOV. The peaks shifted by 1/TR relative to these are neglected. This is a good approximation as the transverse magnetization falls off with $1/\omega$ around a peak's central frequency.

3.2. Evolution into the steady-state

To determine the number of startup-cycles to reach steady-state in an experiment the higher order terms of M_{xy} need to be considered. As illustrated in Fig. 4, magnetization builds up exponentially with $T2$ and subsequently decays slowly towards steady-state with $T1$. Depending on the actual applications, data sampling may thus be started after two to three times $T2$.

3.3. Experiments

The experiments were performed on 3.0 T Achieva and 1.5 T Intera whole body MR systems (Phillips Medical Systems, Best, The Netherlands). A conventional Cartesian SSFP sequence was used with the phase-alternation removed and the flip-angle function implemented into the software (Fig. 2). For data acquisition a standard segmented acquisition scheme was adapted such that multiple k-space profiles could be collected at different times in the periodicity TS of the steady-state.

After acquisition the data were exported as raw data to a computer and reconstructed with Matlab (MathWorks, Natick, MA) using the data phasing formulas as given in Appendix C.

3.4. Phantom measurements

Phantom experiments were carried out on a spherical phantom filled with distilled water using the body coil for signal transmission and reception. After shimming the volume of interest, a gradient of 0.12 mT/m was set in z-direction in the magnet, thereby overlaying the z-axis with a frequency-axis. All images were acquired as single-slice, matrix 256×256, $\mathrm{TR} = 3.54$ ms, $\mathrm{TE} = \mathrm{TR}/2$, $\mathrm{TS} = 181$ ms and $\alpha_0 = 0.08°$. Acquisition time was 51 s including dismissed 1000 start-up shots.

In the first experiment 51 peaks were excited such that the entire frequency-FOV of 1/TR was covered. In the second experiment the spectral field-of-view was reduced by a spectral field-of-view reduction factor of 2; 51 peaks were excited with $\mathrm{TS} = 361$ ms. The peaks are shifted towards each other by the spectral field-of-view reduction factor and TS is likewise two times as long as in the first experiment. All other parameters, including the acquisition time, were identical.

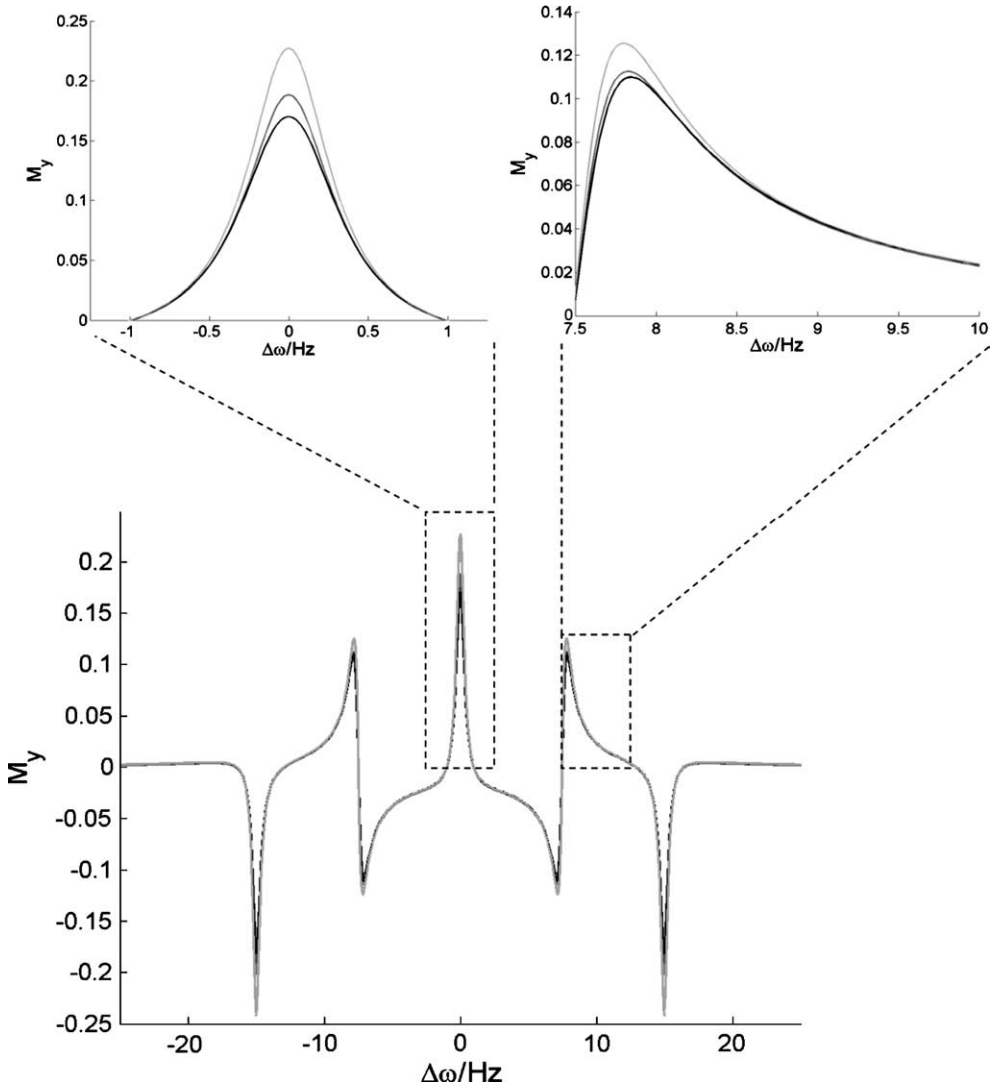

Fig. 3. Frequency response and comparison of second order perturbation solution (light gray line), pulse-sequence simulated by rotational matrices (gray line) and third order perturbation solution (black line) after the evolution of 3/4TS sequence time. Pulses are applied about x-axis using following flip function, $\omega_{xy}(t) = \alpha_0 \sum_{j=-2}^{2} \cos(15\pi jt/\sec) \sum_{i=0}^{\infty} \delta(t - i\mathrm{TR})$, parameters: $T1 = 2$ s, $T2 = 0.5$ s, $\mathrm{TR} = 4$ ms, $\mathrm{TS} = 133$ ms, $\alpha_0 = 0.11°$. The flip-angle for optimal excitation of one peak is $\alpha_0 = 0.23°$.

The flip-functions for the experiment were

$$\omega_{xy}(t) = \alpha_0 \sum_{j=-25}^{25} \cos\left(\frac{2\pi}{\mathrm{TS}} jt\right) \sum_{i=0}^{\infty} \delta(t - i\mathrm{TR}). \tag{11}$$

The flip-function is real and therefore all pulses are applied about one axis. For slice-selection sinc-Gaussian pulses with a bandwidth of more than an order of magnitude larger than the excited band of peaks were used. Thereby the frequency-selectivity of the pulses does not need to be taken into account when describing the equilibrium.

3.5. In vivo measurements

The knee of a healthy volunteer was examined using a birdcage knee coil for signal reception and the body coil for excitation. These measurements were performed on a 1.5 T Phillips Intera system. The images were acquired as single slice with a 256×256 matrix, $\mathrm{TR} = 6.8$ ms, $\mathrm{TE} = \mathrm{TR}/2$, $\mathrm{TS} = 632$ ms, $\alpha_0 = 0.5°$ and $\mathrm{SAR} = 0.1$ W/kg. Acquisition time was 58 s including 100 dismissed start-up shots.

The images were acquired with 31 peaks and a spectral field-of-view reduction factor of 3. The flip-function was

$$\omega_{xy}(t) = \alpha_0 \sum_{j=-15}^{15} \cos\left(\frac{2\pi}{\mathrm{TS}} jt\right) \sum_{i=0}^{\infty} \delta(t - i\mathrm{TR}) \tag{12}$$

with the same sinc-Gaussian slice selection pulses as used in the phantom measurements. The images were reconstructed as the absolute values of the summed absorption components of the 31 excited peaks.

For the water image, the excitation peaks were centered around the water frequency, while for the fat image the frequency was offset by 220 Hz.

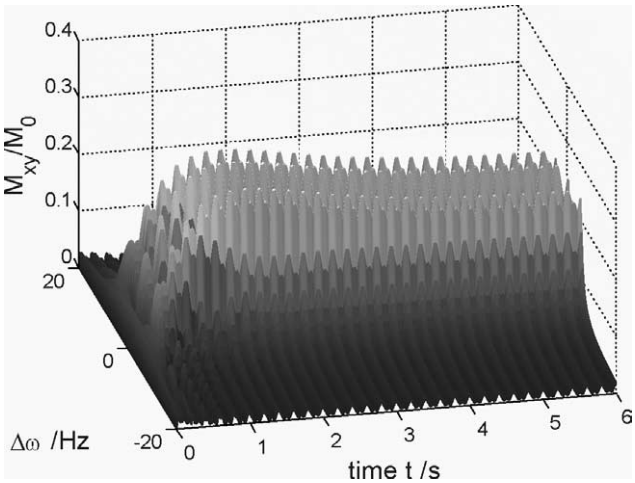

Fig. 4. Time evolution to the steady state, simulation with rotational matrices, pulses applied about x'-axis. The signal rises exponentially with $T2$ and then decays to a slightly smaller value, as the M_z magnetization reaches its equilibrium value. After the steady-state is reached, the oscillation in the magnitude of the peaks is due to the rotation of the peaks against each other. Parameters are: $T1 = 2$ s, $T2 = 0.5$ s, TR = 2 ms, $\omega(t) = \alpha_0 \sum_{j=-1}^{1} \cos(10\pi jt/\text{sec}) \sum_{i=0}^{\infty} \delta(t - i\text{TR}), \alpha_0 = 0.11°$.

4. Results

4.1. Phantom experiments

4.1.1. 51 peaks, spectral field-of-view reduction factor 1

The frequency-axis in z-direction maps the peaks onto the left–right direction of the image. As the field-shift over the entire slice through the sphere is larger than 1/TR, side peaks can be seen in the images. Fig. 5 demonstrates this. As the image was acquired at TE = TR/2 the side peaks are rotated 180° relative to the primary ones and create the (negative) dark areas. Fig. 5B shows the sum of the dispersive components which cancel each other to a large degree and create a slope over the primary peak region. Figs. 5C and D show the absorption and dispersion components of the 25th peak, respectively.

The imperfections in the profiles are due to local B0-inhomogeneities and phases in the acquired data from excitation and reception.

4.1.2. 51 peaks, spectral field-of-view reduction factor 2

To demonstrate that the principle also works with a spectral field-of-view reduction factor different from $c = 1$ another measurement was conducted using the same setup and an identical gradient in z-direction. The results can be seen in Fig. 6.

4.2. In vivo measurements

To demonstrate the in vivo applicability water- and fat-selective knee images of a healthy volunteer were acquired (Fig. 7). It is seen that the different water and fat compartments in the knee are discriminated well. It is to be noted, however, that tissue components with short relaxation times appear brighter as compared to results obtained with conventional gradient echo techniques given the shorter echo-time employed with the present method.

5. Discussion

A mathematical framework to design small flip-angle pulse sequences for steady-state excitation has been presented. By using a second order analytical description of the magnetization, a desired spectral response can be designed by applying a periodic flip angle function. Using sequences employing balanced gradients for spatial encoding, chemical shift imaging can be achieved. These sequences have the unique ability to excite and resolve only part of the spectrum with a high resolution without selective pulses and at extremely low SAR. In the chosen frequency interval, the signal strength can reach the same amplitude as the one obtained with balanced SSFP employing strong excitation.

To resolve m of the peaks, k_ω-space is to be sampled m times within TS, resulting in a frequency-field of view of $1/\text{TR} = m/\text{TS}$. This potentially allows resolving one peak in each spatial "voxel" with a maximum bandwidth of 1/TR. The concepts of spectral resolution and voxels have to be carefully considered for the proposed sequence. In contrast to conventional CSI imaging, a comb instead of a band of frequencies is excited. Accordingly, resolution corresponds to the density of excited frequencies in the comb. High spectral resolution requires long sequence repetition times TS analogous to longer sampling of the FID in conventional CSI imaging. It follows that the width of a spectral "voxel" scales with 1/TS. However, since the linewidth of excited frequencies remains unchanged at $1/T2$ in first approximation, regardless of TS, the excited region may be smaller than the width of a spectral "voxel."

As the framework proposed holds within the limits of weak excitation only, the flip angle, which is a function of the relaxation properties, is a critical parameter. Accordingly, accurate power adjustment on the system used is necessary to obtain optimal results. Likewise, a good estimation of relaxation properties of the tissue to be imaged is important.

Amplifier nonlinearities will cause inaccuracies in the excitation strength of peaks. The effect of erroneous excitation is given by the Fourier series of the difference between applied and intended flip-function (Eq. (8)). RF linearity proved sufficient for water fat images of the knee, but further investigations are warranted for applications such as spectroscopic imaging in the presence of a large water signal. Spurious excitation peaks may result in artefacts. To prevent these spurious peaks from folding into the spectrum one may chose to acquire the entire spectral FOV at the expense of longer measurement times at a given spectral resolution.

In terms of current practical limitations, it is to be noted that clinical MR systems available today may exhibit considerable drifts of the resonance frequency due to temperature shifts in the passive steel shims. This, however, may be accounted for by frequency locking methods as available

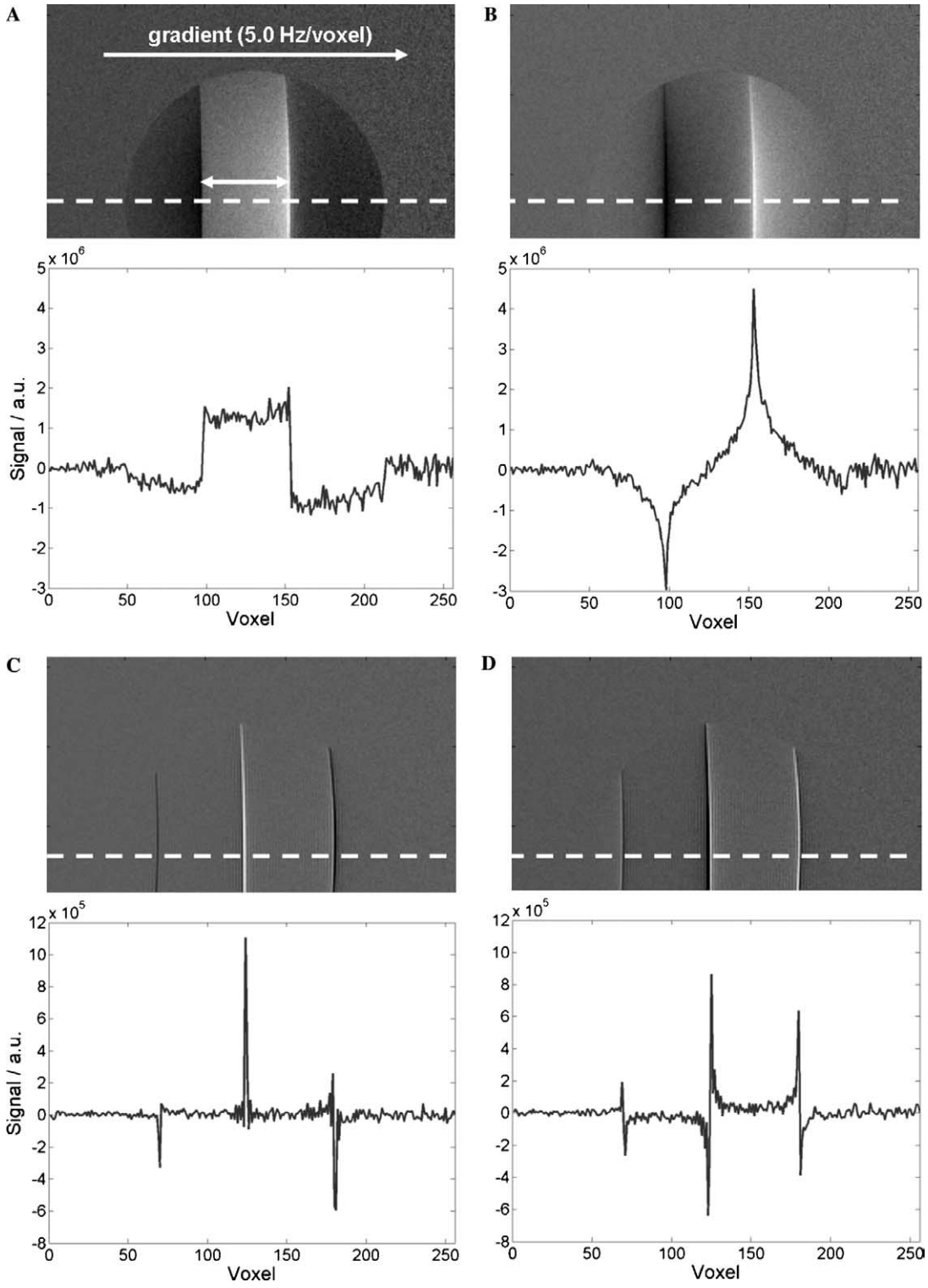

Fig. 5. Phantom experiment with 51 peaks and spectral field-of-view reduction factor 1. The plots show the profiles through the images at the dotted line. (A) Sum of the real image component. The white arrow shows the distance 1/TR on the frequency axis between two peaks. (B) Sum of the imaginary image components. (C) Absorption (real) component of peak 25. (D) Dispersion (imaginary) component of peak 25.

on NMR equipment. Stronger B0-inhomogeneity requires a wider range of frequencies to be excited and read out.

Potential SNR gains relative to existing methods strongly depend on relaxation properties of tissue and the specific parameters used in an experiment. In theory, the method presented permits for signal levels comparable to conventional SSFP, which should outperform non-refocused methods in most cases.

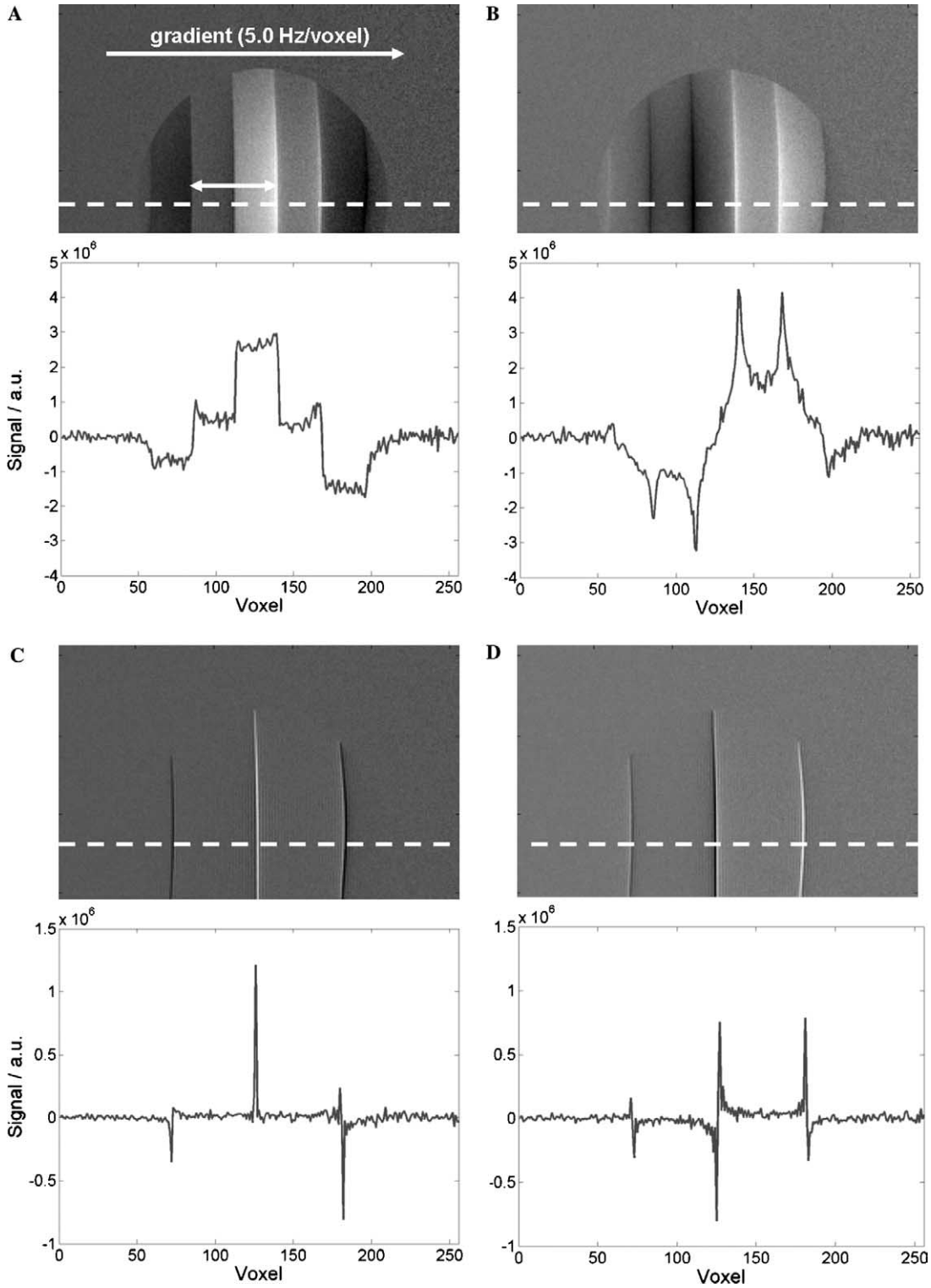

Fig. 6. Phantom experiment with 51 excited peaks and a spectral field-of-view reduction factor of 2. The plots show the profiles of the images at the dotted line. (A) Sum of the real image components. The white arrow shows the distance 1/TR on the frequency axis between two peaks. A residual amount of signal can be seen between the excited bands due to imperfections in the phase of the coil over the object. Therefore only the center peak is phased correctly. (B) Sum of the imaginary image components. (C) Absorption (real) signal of peak 25. (D) Dispersion (imaginary) component of peak 25.

The sequence is optimally suited for spectroscopic imaging, allowing the reduction of the acquired spectral field-of-view for imaging time. This permits sampling a high spatial resolution with only few spectral points at high SNR. As SI applications are generally limited by SNR, this is highly desirable. The very low SAR can make this technique interesting for extremely high field strengths.

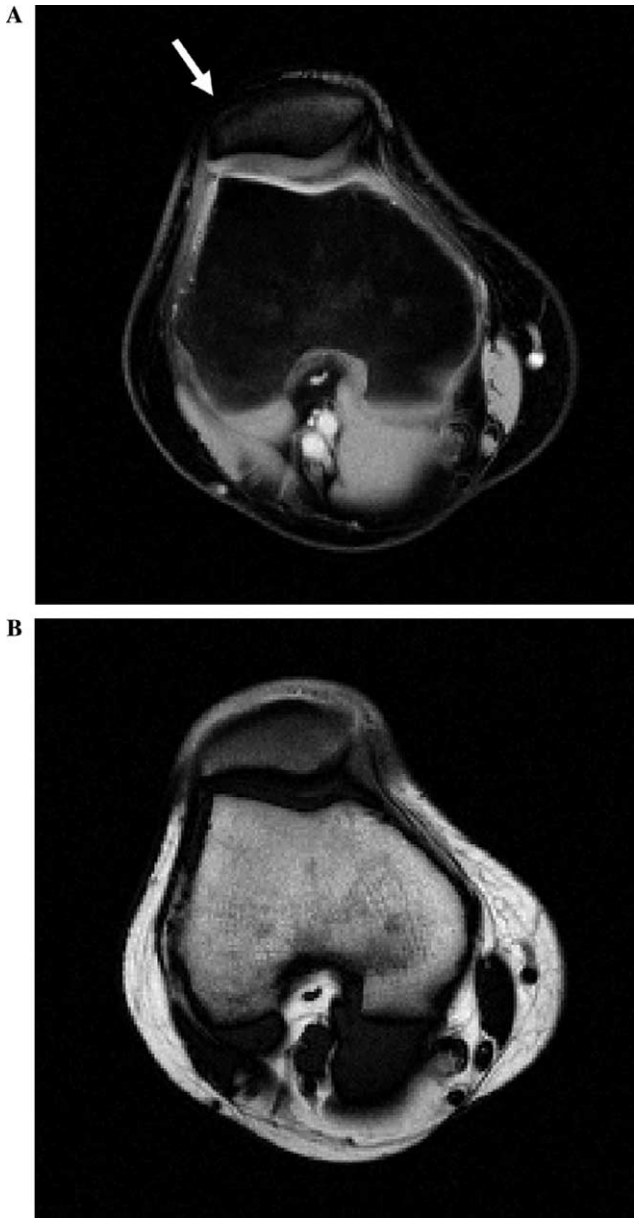

Fig. 7. Images of right knee of healthy volunteer. The images were reconstructed from the summation of the absorption components of 31 excited peaks. In the separate acquisitions a 50 Hz interval was excited with a uniform excitation strength of $\alpha_0 = 0.5°$ around the water frequency in the water image (A), and with a frequency offset of −220 Hz for the fat image (B). It is seen that the excited frequency interval of 50 Hz was not sufficient to fully compensate for the full range of field inhomogeneities encountered across the knee. Accordingly a small area of signal void can be seen at the top (arrow).

6. Conclusion

A new type of steady-state frequency selective imaging employing low excitation has been presented. Based on a mathematical framework, the frequency response can be designed by weighting a periodic flip angle function. The method holds considerable promise in particular for high field in vivo imaging where power deposition presents a severe limitation to conventional large flip angle sequences with short repetition times.

Acknowledgments

The authors thank the SEP program of the ETH Zurich, Grant No. TH7/02-2 and Phillips Medical Systems, Best, The Netherlands for financial support.

Appendix A

The differential equations deduced above are:

$$\begin{aligned}
&\tfrac{\mathrm{d}}{\mathrm{d}t}M_{xy}^{(0)}(t) = aM_{xy}^{(0)}(t) && \tfrac{\mathrm{d}}{\mathrm{d}t}M_{z}^{(0)}(t) = -\tfrac{M_z^{(0)}(t)}{T1} + \tfrac{M_o}{T1}\\
&\tfrac{\mathrm{d}}{\mathrm{d}t}M_{xy}^{(1)}(t) = aM_{xy}^{(1)}(t) && \tfrac{\mathrm{d}}{\mathrm{d}t}M_{z}^{(1)}(t) = Im(ib(t)\\
&\qquad +b(t)M_z^{(0)}(t) && \qquad \times M_{xy}^{(0)}(t)) - \tfrac{M_z^{(1)}(t)}{T1}\\
&\vdots && \vdots\\
&\tfrac{\mathrm{d}}{\mathrm{d}t}M_{xy}^{(m)}(t) = aM_{xy}^{(m)}(t) && \tfrac{\mathrm{d}}{\mathrm{d}t}M_{z}^{(m)}(t) = Im(ib(t)\\
&\qquad +b(t)M_z^{(m-1)}(t) && \qquad \times M_{xy}^{(m-1)}(t)) - \tfrac{M_z^{(m)}(t)}{T1}
\end{aligned} \tag{13}$$

These equations can be solved sequentially

$$\begin{aligned}
&\frac{\mathrm{d}}{\mathrm{d}t}y = c(t)y + d(t) \to y(t)\\
&\quad = \mathrm{e}^{G(t)}\left[y(\xi) + \int_\xi^t d(\tau)\mathrm{e}^{-G(\tau)}\mathrm{d}\tau\right]
\end{aligned} \tag{14}$$

with $G(\tau) = \int_\xi^\tau c(t)\mathrm{d}t$ and the initial condition $y(\xi)$ at the starting time ξ.

The zeroth order in M_{xy} and M_z equates to:

$$M_{xy}^{(0)}(t) = M_{xy}^{(0)}(\xi)\mathrm{e}^{a(t-\xi)} = 0, \tag{15}$$

$$\begin{aligned}
M_z^{(0)}(t) &= \mathrm{e}^{-(t-\xi)/T1}\left[M_z^{(0)}(\xi) + \int_\xi^t \frac{M_0}{T1}\mathrm{e}^{(\tau-\xi)/T1}d\tau\right]\\
&= \mathrm{e}^{-(t-\xi)/T1}\left[M_z^{(0)}(\xi) + M_0(\mathrm{e}^{(t-\xi)/T1} - 1)\right]\\
&= M_0 + (M_z^{(0)}(\xi) - M_0)\mathrm{e}^{-(t-\xi)/T1} = M_0
\end{aligned} \tag{16}$$

with the initial conditions $M_{xy}^{(0)}(\xi) = 0$, $M_z^{(0)}(\xi) = M_0$, $\xi = 0$.

The first order in M_{xy} and M_z calculates to:

$$\begin{aligned}
M_{xy}^{(1)}(t) &= \mathrm{e}^{a(t-\xi)}\left[M_{xy}^{(1)}(\xi) + \int_\xi^t b(t)M_z^{(0)}(t)\mathrm{e}^{-a(\tau-\xi)}\mathrm{d}\tau\right]\\
&= \mathrm{e}^{a(t-\xi)}\left[M_{xy}^{(1)}(\xi) + M_0\sum_\Omega b_\Omega\int_\xi^t \mathrm{e}^{\mathrm{i}\Omega\tau - a(\tau-\xi)}\mathrm{d}\tau\right]\\
&= \mathrm{e}^{a(t-\xi)}\left[M_{xy}^{(1)}(\xi) + M_0\sum_\Omega \frac{b_\Omega}{\mathrm{i}\Omega - a}(\mathrm{e}^{\mathrm{i}\Omega t - a(t-\xi)} - \mathrm{e}^{\mathrm{i}\Omega\xi})\right]\\
&= M_{xy}^{(1)}(\xi)\mathrm{e}^{a(t-\xi)} + M_0\sum_\Omega \frac{b_\Omega}{\mathrm{i}\Omega - a}(\mathrm{e}^{\mathrm{i}\Omega t} - \mathrm{e}^{at}\mathrm{e}^{(\mathrm{i}\Omega - a)\xi})\\
&= M_0\sum_\Omega \frac{b_\Omega}{\mathrm{i}\Omega - a}(\mathrm{e}^{\mathrm{i}\Omega t} - \mathrm{e}^{at})
\end{aligned} \tag{17}$$

with $b(t) = \sum_\Omega b_\Omega e^{i\Omega t}, M_{xy}^{(1)}(\xi) = 0,\ \xi = 0.$

$$M_z^{(1)}(t) = e^{-(t-\xi)/T1}\left[M_z^{(1)}(\xi) + \int_\xi^t Im(ib(t)M_{xy}^{(0)}(t))e^{(\tau-\xi)/T1}d\tau\right] = e^{-(t-\xi)/T1}M_z^{(1)}(\xi) = 0 \quad (18)$$

with $b(t) = \sum_\Omega b_\Omega e^{i\Omega t},\ M_{xy}^{(1)}(\xi) = 0,\ \xi = 0.$

The second order in M_{xy} and M_z becomes

$$M_{xy}^{(2)}(t) = e^{a(t-\xi)}\left[M_{xy}^{(2)}(\xi) + \int_\xi^t b(t)M_z^{(1)}(t)e^{-a(\tau-\xi)}d\tau\right] = e^{a(t-\xi)}M_{xy}^{(2)}(\xi) = 0 \quad (19)$$

as $M_{xy}^{(2)}(\xi) = 0,\ \xi = 0$

$$M_z^{(2)}(t) = e^{-(t-\xi)/T1}\left[M_z^{(2)}(\xi) + \int_\xi^t Im(ib(t)M_{xy}^{(1)}(t))e^{(\tau-\xi)/T1}d\tau\right] \quad (20)$$

with $M_z^{(2)}(\xi) = 0,\ \xi = 0$ results in

$$\begin{aligned} M_z^{(2)}(t) &= e^{-t/T1}\int_0^t \frac{1}{2i}(ib(t)M_{xy}^{(1)}(t) - (ib(t)M_{xy}^{(1)}(t))^*)e^{\tau/T1}d\tau \\ &= \frac{1}{2}e^{-t/T1}\int_0^t (b(t)M_{xy}^{(1)}(t) + b^*(t)M_{xy}^{(1)*}(t))e^{\tau/T1}d\tau \\ &= m^{(2)}(t) + m^{(2)*}(t), \end{aligned} \quad (21)$$

where $*$ denotes that the complex conjugate is taken, with

$$\begin{aligned} m^{(2)}(t) &= \frac{1}{2}e^{-t/T1}\int_0^t b(t)M_{xy}^{(1)}(t)e^{\tau/T1}d\tau \\ &= \frac{1}{2}e^{-t/T1}\sum_{\Omega,\Omega'} C_\Omega b_{\Omega'}\int_0^t e^{(i(\Omega+\Omega')+1/T1)\tau} - e^{(i\Omega'+a+1/T1)\tau}d\tau \\ &= \frac{1}{2}e^{-t/T1}\sum_{\Omega,\Omega'} C_\Omega b_{\Omega'}\left[\frac{e^{(i(\Omega+\Omega')+1/T1)t}-1}{1/T1+i(\Omega+\Omega')} - \frac{e^{(i\Omega'+a+1/T1)t}-1}{1/T1+i\Omega'+a}\right] \\ &= \frac{1}{2}\sum_{\Omega,\Omega'} C_\Omega b_{\Omega'}\left[\frac{e^{i(\Omega+\Omega')t}-e^{-t/T1}}{1/T1+i(\Omega+\Omega')} - \frac{e^{(i\Omega'+a)t}-e^{-t/T1}}{1/T1+i\Omega'+a}\right] \end{aligned} \quad (22)$$

with

$$k_1 = \frac{1}{2}\frac{1}{\frac{1}{T1}+i(\Omega+\Omega')} \text{ and } k_2 = \frac{1}{2}\frac{1}{\frac{1}{T1}+a+i\Omega'}$$

$$M_z^{(2)}(t) = = 2Re\left\{\sum_{\Omega,\Omega'} C_\Omega b_{\Omega'}[k_1(e^{i(\Omega+\Omega')t}-e^{-t/T1}) - k_2(e^{(i\Omega'+a)t}-e^{-t/T1})]\right\} \quad (23)$$

Third order in M_{xy}

$$\begin{aligned} M_{xy}^{(3)}(t) &= e^{a(t-\xi)}\left[M_{xy}^{(3)}(\xi) + \int_\xi^t b(t)M_z^{(2)}(t)e^{-a(\tau-\xi)}d\tau\right] \\ &= e^{at}\int_0^t b(t)(m^{(2)}(t)+m^{(2)*}(t))e^{-a\tau}d\tau \\ &= e^{at}\int_0^t b(t)m^{(2)}(t)e^{-a\tau}d\tau + e^{at}\int_0^t b(t)m^{(2)*}(t)e^{-a\tau}d\tau \end{aligned} \quad (24)$$

as $M_{xy}^{(3)}(\xi) = 0,\ \xi = 0.$

The first term can be rewritten as

$$\begin{aligned} &e^{at}\sum_{\Omega,\Omega',\Omega''} C_\Omega b_{\Omega'}b_{\Omega''}\int_0^t e^{i\Omega''\tau}e^{-a\tau}[k_1(e^{i(\Omega+\Omega')\tau}-e^{-\tau/T1}) \\ &-k_2(e^{(i\Omega'+a)\tau}-e^{-\tau/T1})]d\tau \\ &= e^{at}\sum_{\Omega,\Omega',\Omega''} C_\Omega b_{\Omega'}b_{\Omega''}\left[k_1\left(\frac{e^{(i(\Omega+\Omega'+\Omega'')-a)t}-1}{-a+i(\Omega+\Omega'+\Omega'')} - \frac{e^{(i\Omega''-1/T1-a)t}-1}{i\Omega''-a-1/T1}\right) - k_2\left(\frac{e^{i(\Omega'+\Omega'')t}-1}{i(\Omega'+\Omega'')} - \frac{e^{(i\Omega''-1/T1-a)t}-1}{i\Omega''-a-1/T1}\right)\right] \\ &= \sum_{\Omega,\Omega',\Omega''} C_\Omega b_{\Omega'}b_{\Omega''}\left[k_1\left(\frac{e^{i(\Omega+\Omega'+\Omega'')t}-e^{at}}{-a+i(\Omega+\Omega'+\Omega'')} - \frac{e^{(i\Omega''-1/T1)t}-e^{at}}{i\Omega''-a-1/T1}\right) - k_2\left(\frac{e^{(i(\Omega'+\Omega'')+a)t}-e^{at}}{i(\Omega'+\Omega'')} - \frac{e^{(i\Omega''-1/T1)t}-e^{at}}{i\Omega''-a-1/T1}\right)\right]. \end{aligned} \quad (25)$$

The second term is

$$\begin{aligned} &e^{at}\sum_{\Omega,\Omega',\Omega''} C_\Omega^* b_{\Omega'}^* b_{\Omega''}\int_0^t e^{i\Omega''\tau}e^{-a\tau}[k_1^*(e^{-i(\Omega+\Omega')\tau}-e^{-\tau/T1}) \\ &-k_2^*(e^{(-i\Omega'+a^*)\tau}-e^{-\tau/T1})]d\tau \\ &= \sum_{\Omega,\Omega',\Omega''} C_\Omega^* b_{\Omega'}^* b_{\Omega''}\left[k_1^*\left(\frac{e^{i(\Omega''-\Omega-\Omega')t}-e^{at}}{-a+i(\Omega''-\Omega-\Omega')} - \frac{e^{(i\Omega''-1/T1)t}-e^{at}}{i\Omega''-a-1/T1}\right) - k_2^*\left(\frac{e^{(i(\Omega''-\Omega')+a^*)t}-e^{at}}{i(\Omega''-\Omega')+a^*-a} - \frac{e^{(i\Omega''-1/T1)t}-e^{at}}{i\Omega''-a-1/T1}\right)\right] \end{aligned} \quad (26)$$

Resulting in

$$\begin{aligned} M_{xy}^{(3)}(t) = &\sum_{\Omega,\Omega',\Omega''} C_\Omega b_{\Omega'}b_{\Omega''}\left[k_1\left(\frac{e^{i(\Omega+\Omega'+\Omega'')t}-e^{at}}{-a+i(\Omega+\Omega'+\Omega'')} - \frac{e^{(i\Omega''-1/T1)t}-e^{at}}{i\Omega''-a-1/T1}\right) - k_2\left(\frac{e^{(i(\Omega'+\Omega'')+a)t}-e^{at}}{i(\Omega'+\Omega'')} - \frac{e^{(i\Omega''-1/T1)t}-e^{at}}{i\Omega''-a-1/T1}\right)\right] \\ &+ \sum_{\Omega,\Omega',\Omega''} C_\Omega^* b_{\Omega'}^* b_{\Omega''}\left[k_1^*\left(\frac{e^{i(\Omega''-\Omega-\Omega')t}-e^{at}}{-a+i(\Omega''-\Omega-\Omega')} - \frac{e^{(i\Omega''-1/T1)t}-e^{at}}{i\Omega''-a-1/T1}\right) - k_2^*\left(\frac{e^{(i(\Omega''-\Omega')+a^*)t}-e^{at}}{i(\Omega''-\Omega')+a^*-a} - \frac{e^{(i\Omega''-1/T1)t}-e^{at}}{i\Omega''-a-1/T1}\right)\right]. \end{aligned} \quad (27)$$

In steady-state this reduces to

$$M_{xy}^{(3)}(t) = \sum_{\Omega,\Omega',\Omega''} C_\Omega b_{\Omega'} b_{\Omega''} \frac{e^{i(\Omega+\Omega'+\Omega'')t}}{-a+i(\Omega+\Omega'+\Omega'')} + \sum_{\Omega,\Omega',\Omega''} C_\Omega^* b_{\Omega'}^* b_{\Omega''} k_1^* \frac{e^{i(\Omega''-\Omega-\Omega')t}}{-a+i(\Omega''-\Omega-\Omega')}$$
$$= \sum_{\Omega,\Omega',\Omega''} b_{\Omega''} e^{i\Omega''t} \left[C_\Omega b_{\Omega'} k_1 \frac{e^{i(\Omega+\Omega')t}}{-a+i(\Omega+\Omega'+\Omega'')} + C_\Omega^* b_{\Omega'}^* k_1^* \frac{e^{-i(\Omega+\Omega')t}}{-a+i(\Omega''-\Omega-\Omega')} \right] \quad (28)$$

Comment. Some terms of the sum written as it is diverge for $\Omega' + \Omega'' = 0$. This does not happen if one performs the integration of these terms separately, resulting in terms proportional to te^{at}. These terms do not contribute to the steady-state.

Appendix B. Discretization of flip function

The effect of δ-like pulses in flip functions is presented.

If infinitely short δ-pulses are applied at a repetition rate TR, the rotation about the x- and y-axes can be written as

$$\omega_{xy}(t) = \alpha(t) \sum_{n=-\infty}^{\infty} \delta(t - n\mathrm{TR}). \quad (29)$$

The Fourier coefficients of this periodic function can be derived with the convolution theorem

$$\omega_{xy_\Omega} = \{\omega_{xy}(t)\}_\Omega = \left\{ \alpha(t) \sum_{n=-\infty}^{\infty} \delta(t - n\mathrm{TR}) \right\}_\Omega = \alpha_\Omega * \left\{ \sum_{n=-\infty}^{\infty} \delta(t - n\mathrm{TR}) \right\}_\Omega . \quad (30)$$

The brackets denote that the Fourier-conjugate of the contained function is taken with respect to the rotational frequency Ω. With a pulse sequence, where the N pulses are repeated every $\mathrm{TS} = N{\cdot}\mathrm{TR}$, the Fourier series coefficients of the δ-comb are given by

$$\left\{ \sum_{n=-\infty}^{\infty} \delta(t - n\mathrm{TR}) \right\}_{\Omega=2\pi\frac{k}{\mathrm{TS}}} = \frac{1}{\mathrm{TS}} \int_0^{\mathrm{TS}} \sum_{n=-\infty}^{\infty} \delta(t - n\mathrm{TR}) \times e^{-i2\pi\frac{k}{\mathrm{TS}}t} dt$$
$$= \frac{1}{TS} \left(\sum_{n=1}^{N-1} e^{-i2\pi\frac{k}{\mathrm{TS}}n\mathrm{TR}} + \frac{1}{2} + \frac{1}{2} e^{-i2\pi\frac{k}{\mathrm{TS}}\mathrm{TS}} \right)$$
$$= \frac{1}{\mathrm{TS}} \sum_{n=0}^{N-1} e^{-i2\pi\frac{k}{\mathrm{TS}}n\mathrm{TR}} = \frac{N}{2\pi} \delta_{k \bmod N, 0} \quad (31)$$

with a Kronecker-delta δ_{ij}. Applying the discrete convolution in Eq. (30) results in

$$\omega_{xy_{\Omega=2\pi\frac{j}{\mathrm{TS}}}} = \sum_k \alpha_{2\pi\frac{k}{\mathrm{TS}}} \left\{ \sum_{n=-\infty}^{\infty} \delta(t - n\mathrm{TR}) \right\}_{2\pi\frac{j-k}{\mathrm{TS}}} = \frac{N}{\mathrm{TS}} \sum_{k \bmod N = \Omega} \alpha_{2\pi\frac{k}{\mathrm{TS}}}. \quad (32)$$

This result shows that application of a δ-like pulse at a constant repetition rate results in N remaining independent coefficients of the flip-function Fourier series. The excitation profile is periodic with 1/TR, due to the fact that the response in the rotating frame of reference is equivalent for all frequencies shifted by 1/TR to each other. This effect is analogous to the Nyquist sampling criterion in that only a finite number N of frequencies are relevant

$$\omega_{xy}(t) = \sum_{k=-\infty}^{+\infty} \alpha_{2\pi\frac{k}{\mathrm{TS}}} e^{i2\pi\frac{k}{\mathrm{TS}}t} = \sum_{j=0}^{n-1} \left(\sum_{j=k \bmod n} \alpha_k \right) e^{i2\pi\frac{j}{\mathrm{TS}}t} \quad (33)$$

An analogous calculation can be performed for other pulse shapes, for instance of the slice-selection pulses used in the experiments (not shown here).

Appendix C. Data reconstruction

For the following derivation it is assumed that data were acquired during steady-state. If many peaks are excited at the same time, one will need to differentiate between them once the data have been acquired. Given that the signal was sampled N times within TS (after each excitation pulse) at times $t_n = t_0 + n\Delta t$ and using Eq. (8) the selection profile can be written as

$$M_{xy}(t_n) = \sum_{j=0}^{N-1} C_{\Omega=2\pi\frac{j}{\mathrm{TS}}} e^{i2\pi\frac{j}{\mathrm{TS}}(t_0+n\Delta t)} = \sum_{j=0}^{N-1} C_{2\pi\frac{j}{\mathrm{TS}}} e^{i\varphi_j} e^{i2\pi\frac{n}{N}j} \text{ with } \varphi_j = 2\pi\frac{t_0}{T_s}j, \quad \Delta t = \frac{\mathrm{TS}}{N}. \quad (34)$$

The single Lorentzian peak k in the frequency domain can thereby be resolved by a discrete Fourier transformation

$$\sum_{n=0}^{N-1} M_{xy}(t_n) e^{-i2\pi\frac{n}{N}k} = \sum_{j=0}^{N-1} C_{2\pi\frac{j}{\mathrm{TS}}} e^{i\varphi_j} \sum_{n=0}^{N-1} e^{i2\pi\frac{n}{N}(j-k)} = \sum_{j=0}^{N-1} C_{2\pi\frac{j}{\mathrm{TS}}} e^{i\varphi_j} N\delta_{jk} = NC_{2\pi\frac{j}{\mathrm{TS}}} e^{i\varphi_k}. \quad (35)$$

It follows that a maximum of $\mathrm{TS}/\mathrm{TR} = N$ peaks can be detected over the spectral field-of-view 1/TR.

C.1. Reduction of the spectral field-of-view

If only a portion of the spectral field-of-view is excited, i.e., $m = N/c$ neighboring peaks are selected with c denoting the field-of-view reduction-factor, the reconstruction cannot directly be performed using Eq. (35). Instead, the single Lorentzian peak k in the frequency domain can be resolved by the following transformation on a dataset of k-space data $n + kc$, with $k = 0, 1, \ldots, m - 1$

$$\sum_{k=0}^{m-1} e^{i2\pi b\frac{n+kc}{N}} e^{-i2\pi a\frac{kc}{N}} = e^{i2\pi\frac{n}{N}} \sum_{k=0}^{m-1} e^{i2\pi\frac{kc}{N}(b-a)}$$
$$= e^{i2\pi\frac{n}{N}} \sum_{k=0}^{m-1} e^{i2\pi\frac{k}{m}(b-a)}$$
$$= m e^{i2\pi\frac{n}{N}} \delta_{0,(b-a)\bmod m} \quad (36)$$

and using the relation of the discrete Fourier transformation

$$\sum_{k=0}^{m-1} e^{i2\pi b\frac{k}{m}} \cdot e^{-i2\pi a\frac{k}{m}} = m \cdot \delta_{0,(a-b)\bmod m}. \quad (37)$$

Thus

$$\sum_{k=0}^{m-1} M_{xy}(t_n) e^{-i2\pi\frac{n}{N}k} = \sum_{j=0}^{m-1} C_{2\pi\frac{j}{TS}} e^{i\varphi_j} \sum_{k=0}^{m-1} e^{i2\pi\frac{n}{N}(j-k)}$$
$$= \sum_{j=0}^{m-1} C_{2\pi\frac{j}{TS}} e^{i\varphi_j} m\delta_{0,(j-k)\bmod m}$$
$$= m C_{2\pi\frac{k}{TS}} e^{i\varphi_k}. \quad (38)$$

This allows one to select only a spectral interval of interest, trading the rest of the data for acquisition speed without any loss of spectral resolution. In this case the data must be phased to compensate for signal evolution.

References

[1] G. Bodenhausen, R. Freeman, G.A. Morris, Simple pulse sequence for selective excitation in Fourier-transform NMR, J. Magn. Res. 23 (1976) 171–175.

[2] R. Pohmann, M. von Kienlin, A. Haase, Theoretical evaluation and comparison of fast chemical shift imaging methods, J. Magn. Res. 129 (1997) 145–160.

[3] A. Oppelt, R. Graumann, H. Barfuß, H. Fischer, W. Hartl, W. Schajor, FISP—a new fast MRI sequence, Electromedica (Engl. Ed.) 54 (1986) 15–18.

[4] H.Y. Carr, Steady-state free precession in nuclear magnetic resonance, Phys. Rev. 112 (1958) 1693–1701.

[5] W.R. Overall, D.G. Nishimura, B.S. Hu, Steady-state sequence synthesis and its application to efficient fat-suppressed imaging, Magn. Reson. Med. 50 (2003) 550–559.

[6] S.S. Vasanawala, J.M. Pauly, D.G. Nishimura, Fluctuating equilibrium MRI, Magn. Reson. Med. 42 (1999) 876–883.

[7] S.S. Vasanawala, J.M. Pauly, D.G. Nishimura, Linear combination steady-state free precession MRI, Magn. Reson. Med. 43 (2000) 82–90.

[8] T.Y. Huang, H.W. Chung, F.N. Wang, C.W. Ko, C.Y. Chen, Fat and water separation in balanced steady-state free precession using the Dixon method, Magn. Reson. Med. 51 (2004) 243–247.

[9] B.A. Hargreaves, S.S. Vasanawala, K.S. Nayak, B.S. Hu, D.G. Nishimura, Fat-suppressed steady-state free precession imaging using phase detection, Magn. Reson. Med. 50 (2003) 210–213.

[10] D.I. Hoult, Solution of the Bloch equations in the presence of a varying B1 field—approach to selective pulse analysis, J. Magn. Res. 35 (1979) 69–86.

[11] J.M. Pauly, D.G. Nishimura, A. Macovski, A K-space analysis of small-tip-angle excitation, J. Magn. Res. 81 (1989) 43–56.

[12] G.A. Morris, R. Freeman, Selective excitation in Fourier-transform nuclear magnetic-resonance, J. Magn. Res. 29 (1978) 433–462.

[13] Y. Ke, D.G. Schupp, M. Garwood, Adiabatic Dante sequences for B-1-insensitive narrow-band inversion, J. Magn. Res. 96 (1992) 663–669.

[14] A. Abragam, The Principles of Nuclear Magnetism, Clarendon Press, Oxford, 1961.